Long-term high temperatures affect seed maturation and seed coat integrity in *Brassica napus*

Unnikannan Prabhullachandran[1,2], Ivana Urbánková[3], Alejandro Medaglia-Mata[4,5], Audrey Creff[6], Aline Voxeur[7], Vilma Buršíková[8], Benoit Landrein[6], Jan Hejátko[3], Hélène S. Robert[1]

1. Plant Biotech for stress resilience, Genomics and Proteomics of Plant Systems, Central European Institute of Technology (CEITEC), Masaryk University, Brno, Czech Republic
2. National Centre for Biomolecular Research, Faculty of Science, Masaryk University, Brno, Czech Republic
3. Functional Genomics and Proteomics of Plants, Genomics and Proteomics of Plant Systems, Central European Institute of Technology (CEITEC), Masaryk University, Brno, Czech Republic
4. Bioinformatics Core Facility, Central European Institute of Technology (CEITEC), Masaryk University, Brno, Czech Republic
5. Department of Biology, Faculty of Medicine, Masaryk University, Brno, Czech Republic
6. Laboratoire Reproduction et Développement des Plantes, Université de Lyon, ENS de Lyon, UCB Lyon, CNRS, INRAE, INRIA, Lyon, France
7. Université Paris-Saclay, INRAE, AgroParisTech, Institute Jean-Pierre Bourgin for Plant Science (IJPB), Versailles, France
8. Department of Plasma Physics and Technology, Faculty of Science, Masaryk University, Kotlářská 2, 611 37, Brno, Czech Republic.

Hélène S. Robert (corresponding author helene.robert.boisivon@ceitec.muni.cz)

ORCID

UK 0000-0001-6430-575X

IU 0009-0005-0794-1553

AMM 0000-0003-3496-0571

AC 0000-0001-7736-5882

AV 0000-0001-9452-6756

VB 0000-0001-5505-6632

BL 0000-0002-2371-9996

JH 0000-0002-2622-6046

HSR 0000-0002-6610-836X

Word count 7967

Number of Figures 7

Supporting Information Figures S1-S9 and Tables S1-S2

ABSTRACT

Temperatures above the optimum growth temperature affect seed development; accelerating the embryo development and producing seeds with ruptured seed coats. However, the underlying mechanism of this effect remains unclear. To investigate temperature-induced seed coat rupture, we used a combination of detailed phenotyping, transcriptomics, histology, immunolabelling, cell wall profiling and seed coat mechanics to analyse oilseed rape seeds. Our data suggest that high temperatures accelerate embryo growth, resulting in the formation of larger embryos but not larger seeds. The formation of large embryos increases the mechanical stress exerted on the seed coat cells by the embryo, reducing their thickness. Prolonged exposure to high temperatures during seed development causes the seed coat to mature prematurely, resulting in the accumulation of demethylesterified pectin and making the cell wall more rigid. This inhibits cell growth and limits the expansion of the seed. The consequences of these events result in tension building up in the seed coat cells. These cells eventually undergo seed coat rupture, affecting the quality of the seed. Our work on seed maturation and the mechanism of heat-induced seed coat rupture provides valuable insights for future research into generating thermotolerant *Brassica napus*, crucial in the context of changing climates.

HIGHLIGHTS

- Growth of *Brassica napus* under long-term high temperatures accelerated the embryo growth and led to half of the seeds undergoing seed coat rupture phenotype.
- Pathways linked to cell wall modification were found to be significantly misregulated at high temperatures. The stiffening of the seed coat correlated with increased pectin demethylesterification.
- The faster-growing embryo imparted increased tension to the developing seed coat cells, reducing the thickness of each individual layer. While the seed coat was stiffening, it was unable to restrict the embryo growth, resulting in its rupture.

KEYWORDS

Brassica napus, seed development, cell wall, long-term high temperature, pectin, seed coat rupture, heat stress.

1. INTRODUCTION

The adverse impacts of global warming on agricultural production pose a major challenge to global food security. Extreme weather events, such as heat stress, drought and floods, have the potential to affect the production of staple crops, such as rice, wheat, maize, and soybean (Agnolucci & De Lipsis, 2020; Heino et al., 2023; Jägermeyr et al., 2021; Zhao et al., 2017). The latest average annual global temperature rise in 2025 was 1.19°C above preindustrial levels (Lenssen et al., 2024; *NASA Goddard Institute for Space Studies*, 2026), highlighting the need to adapt agricultural practices to higher temperatures.

Brassica napus (canola or oilseed rape), an allotetraploid species of the Brassicaceae family, is the second most widely cultivated oilseed crop, used for the production of vegetable oil, biofuel, and protein in animal feed. Cultivation of oilseed rape at temperatures above the optimum growth temperature of 21°C for prolonged periods, especially during the flowering stage, resulted in several adverse effects, including rapid vegetative growth, reduced viability of female gametophytes, increased seed abortion rate, accelerated embryo development, and a reduction in seed oil composition (Mácová et al., 2022; Secchi et al., 2023; Young et al., 2004). One of the distinctive phenotypes observed during seed development of certain canola cultivars subjected to prolonged heat stress that affects seed yield is the occurrence of the preharvest sprouting phenotype (Mácová et al., 2022), which is associated with an initial rupture of the seed coat during seed maturation. For our study we termed it as seed coat rupture (SCR) phenotype. The exact mechanism by which this phenotype is regulated at elevated temperatures remains unclear in *Brassica napus*.

In Brassicaceae, seed size is regulated by the interaction between maternal and zygotic signals that coordinate the proper development of the seed coat, endosperm, and embryo (Li et al., 2019). During the maturation of *Arabidopsis* seeds, the pressure generated by the interaction between the developing embryo and the endosperm within the seed, driven by embryo growth, exerts tension on the developing integuments (Creff et al., 2015, 2023). The generated tension is sensed by a specific layer of the seed coat's outer integument (oi), the

96 adaxial epidermis (oi1). This mechanical stimulus triggers a transcriptional response marked
97 by the activation of the mechanosensitive gene *EUI-like P450A1* (*ELA1)*, which is believed to
98 promote cell wall stiffening through demethylesterified pectin accumulation, and thus,
99 regulating seed size (Creff et al., 2023). Cell wall stretching enables the growth of a plant cell
100 which depends on the mechanical strength and dynamic extensibility of the wall (Geitmann
101 & Ortega, 2009). The strength and integrity of the wall during growth is maintained actively
102 by the modification of the cell wall elements (Cosgrove, 2024). The dry mass of the primary
103 plant cell wall is composed of cellulose, hemicellulose, and pectin (Ayala Soto & Serna
104 Saldívar, 2020; Cosgrove, 2024). Pectin forms a hydrated gel-like matrix in which cellulose and
105 hemicellulose cross-link to form the cell wall. It is abundant in the middle lamella, an adhesive
106 layer between adjacent cells. The most abundant pectin, homogalacturonan (HG), is
107 produced in a highly methylesterified state. It can undergo demethylesterification by the
108 activity of pectin methylesterase (PME) based on developmental response (Turbant et al.,
109 2016; Wu et al., 2018; Xu et al., 2022). Blockwise removal of methyl groups can lead to the
110 formation of Ca^{2+} cross-links, which makes the cell wall more rigid and inhibits growth
111 alternatively, random removal can lead to pectin degradation, affecting wall rheology
112 (Bidhendi & Geitmann, 2016; Wu et al., 2018). Seed size correlates with endosperm
113 proliferation and development. The two processes are linked by a brassinosteroid-induced
114 cell expansion and increased levels of methylesterified pectin in the seed coat, which helps to
115 regulate seed size (Lima et al., 2024).
116 In this study, we used a multi-methodology approach to investigate the occurrence of the
117 temperature-induced SCR phenotype. The results show that SCR occurs in seeds around 20
118 days after pollination (20 DAP) when plants are cultivated at elevated temperatures for a
119 prolonged period. The pressure induced by unrestricted embryo growth led to increased
120 tension in the seed coat, characterised by reduced thickness of the seed coat layers, and
121 resulted in early changes in cell wall composition. Accumulation of demethylesterified pectin
122 made the cell wall of the seed coat more rigid inhibiting the cell growth by expansion. It
123 correlates with a reduced elasticity, making the seed coat more prone to rupture. The precise
124 mechanism by which accelerated embryo development influenced by heat stress-mediated
125 seed development in oilseed rape plants remains to be elucidated. A deeper understanding
126 of the effects of prolonged elevated temperatures on seed development could prove

127 invaluable in the generation of thermotolerant varieties of canola varieties, which would help
128 to improve crop yields in the context of global warming in the 21st century.
129
130 **2. MATERIALS AND METHODS**
131 **2.1 Plant materials and growth conditions**
132 *Brassica napus* spring cultivar, Topas DH4079, was used for this study. Seeds were sterilised,
133 germinated, and grown initially in the phytotron (21°C, 16/8 h long day period, 150
134 µmol/m^2/s) until the emergence of the first flowering buds, as previously mentioned (Mácová
135 et al., 2022). Plants were then transferred to greenhouse chambers with control temperature
136 (CT) and heat (HT) conditions maintained under a long-day regime (16/8 h), LED lights with a
137 light intensity of 150 µmol/m^2/s, 35%–45% humidity and temperature of 18°C during the night
138 and ramping to 21°C (CT) and 32°C (HT) during the day. Seeds used for the experiments are
139 obtained from hand-pollinated flowers. The age of the seeds is counted from the day after
140 pollination (DAP).
141
142 **2.2 Seed phenotyping**
143 Roughly ten hand-pollinated and dried siliques from four plants in each of the five biological
144 replicates from CT (n=116) and HT (n=245) conditions were screened for the total, intact
145 (round intact seeds with intact embryo), seeds undergoing SCR (partial or fully ruptured seed
146 coat with intact embryo or germinating embryo respectively) and dead seeds (empty and
147 shrunken without embryo) (Fig. S1a-c). Fresh seeds from 14 to 20 DAP were collected from
148 Topas grown at CT and HT for embryo staging. The whole seed and its isolated embryo were
149 imaged using a Levenhuk M500 base digital camera attached to a Zeiss stemi 305
150 stereomicroscope. Later, the images were used to measure the seed and embryo areas using
151 ImageJ for 14, 18 and 20 DAP. The ratio of the embryo-to-seed area was calculated to get
152 information on the space occupied by the embryo within the seed at each stage of
153 development. Statistical significance was accounted for by a two-way ANOVA test with
154 Tukey's multiple comparisons (* $p < 0.0332$, ** $p < 0.0021$, *** $p < 0.0002$, and **** $p <$
155 0.0001).
156
157 **2.3 RNA extraction and sequencing**

158 RNA was extracted from 50 mg of ground tissue of 14, 18 and 20 DAP intact from CT and HT,
159 and 20 DAP SCR seeds from HT only are collected from three plants in each of the four
160 biological replicates using a NucleoSpin RNA Plant and Fungi kit (Macherey-Nagel) following
161 the manufacturer's protocol. The samples were treated with RNase-free rDNase (Macherey-
162 Nagel) and repurified using the RNeasy MinElute Cleanup Kit (Qiagen). The samples were
163 sequenced by Novogene Genomic Sequencing Labs. After sample quality control and library
164 preparation, paired-end short-read RNA sequencing was performed on poly-A RNA using an
165 Illumina Novaseq Sequencing platform. Quality check of raw paired-end fastq reads was
166 carried out by FastQC (Andrews, 2010), and their origin was categorised using BioBloomTools
167 v2.3.4 (Chu et al., 2014). The Illumina adapters and quality trimming of raw fastq reads were
168 performed using Trimmomatic v0.39 (Bolger et al., 2014) with settings CROP:250 LEADING:3
169 TRAILING:3 SLIDINGWINDOW:4:5 MINLEN:35. Trimmed RNA-Seq reads were mapped to the
170 *Brassica napus* genome (genome build: Bra_napus_v2.0) with gene annotation (NCBI *Brassica*
171 *napus* Annotation Release 101) using STAR v2.7.3a (Dobin et al., 2013) as splice-aware short
172 read aligner and default parameters except outFilterMismatchNoverLmax 0.1 and
173 twopassMode Basic. Quality control after alignment concerning the number and percentage
174 of uniquely- and multi-mapped reads, rRNA contamination, mapped regions, read coverage
175 distribution, strand specificity, gene biotypes, and PCR duplication was performed using
176 RSeQC v4.0.0 (L. Wang et al., 2012), Picard toolkit v2.25.6 (Broad Institute and GitHub
177 Repository, 2018), Qualimap v.2.2.2 (Okonechnikov et al., 2016). All compatible results and
178 statistics were processed by MultiQC v1.10.1 (Ewels et al., 2016). The sequence data have
179 been deposited in the NCBI under the Bio-Project PRJNA1188476
180 (https://www.ncbi.nlm.nih.gov/bioproject/PRJNA1188476).
181 The differential gene expression analysis was calculated based on the gene counts produced
182 using featureCounts from Subread package v2.0 (Liao et al., 2014) and further analysed by
183 Bioconductor package DESeq2 v1.34.0 (Love et al., 2014). Because of its conservative features
184 and to prevent false positive results, data produced by DESeq2 with independent filtering
185 were chosen for the differential gene expression analysis. Genes were considered to be
186 differentially expressed based on a cut-off for adjusted p-value ≤ 0.05 and log2FC ≥1 or ≤-1.
187 The data are compiled in Table S1, Table S2, Fig. S8, and Fig. S9. Clustered heatmaps were
188 generated from selected top differentially regulated genes using R package pheatmap v1.0.12
189 (Kolde, 2015), volcano plots were produced using ggplot2 v3.3.5 package (Wickham, 2011),

190 and MA plots were generated using ggpubr v0.4.0 package (Kassambara, 2018). GO
191 enrichment is done taking all the Entrez gene IDs and cross-mapping them against UniProt
192 IDs, then taking all the transcript sequences and mapping them (using BLAST) against the NCBI
193 Nucleotide database subset for all species under taxons 3701 (A*rabidopsis* genus) and 981071
194 (*Brassicaceae* tribe) obtaining RefSeq gene IDs which were cross-mapped against UniProt IDs
195 and then used in GO enrichment.
196
197 **2.4 Seed embedding and sectioning for seed coat thickness measurements**
198 Seeds were fixed in FAA (45% ethanol, 5% acetic acid and 1.85% formaldehyde) for 24 h under
199 vacuum, followed by another incubation at 4°C for 24 h in fresh FAA. The seeds were washed
200 once with water. Tissue softening was done with Franklin Maceration solution (1:1 v/v of 30%
201 H_2O_2 and glacial acetic acid) for 4 h at 60°C. Dehydration was done using 10, 20, 30, 40, 50,
202 60% ethanol series in 10% glycerine for 1 h at 30°C, followed by 4 days in 70% ethanol at 4°C
203 and dehydration with 80, 90 and 95% ethanol for 1 h at room temperature. Infiltration and
204 embedding with Technovit 7100 (Kulzer Technik Gmbh) were performed according to the
205 manufacturer's protocol with the following modifications. The initial infiltration was
206 performed in a 50% infiltration solution in ethanol overnight at room temperature, followed
207 by incubation for one week at 4°C in 100% infiltration solution with 1% w/v Technovit 7100
208 Hardener I. Embedding was performed with 6.6% w/v Technovit 7100 Hardener II in
209 infiltration solution and incubated for 8 days at -18°C to delay initial polymerisation. The
210 samples were then incubated at room temperature to complete the polymerisation process.
211 The 3-µm sections were prepared with a Leica RM2235 microtome using an attached
212 stainless-steel knife.
213
214 **2.5 Toluidine blue staining**
215 The sections were stained with 0.05% Toluidine blue (Acros Organics) for 1 minute, followed
216 by four washing steps of three minutes each with water. Later the slides were dried on the
217 hot plate maintained at 70°C. Later the slides were mounted in Entellan (Sigma-Aldrich).
218 Imaging of the sections was performed using a Zeiss AxioImager microscope. The thickness of
219 the seed coat layers was measured in twenty regions per section, for three sections per seed
220 and ten seeds per sample, using Image J. Graphs were plotted with significance calculated
221 using a two-way ANOVA test with Tukey multiple comparisons.

222

223 **2.6 Staining of lignin and pectin**

224 Seven seeds at 14 and 18 DAP from CT and HT and 22 DAP only from CT were used. Pectin
225 was detected using a 0.05% w/v Ruthenium Red stain (Sigma-Aldrich) in an aqueous solution.
226 Sections were rehydrated, stained for 7 minutes in Ruthenium Red, followed by two wash
227 steps with water, drying on the hot plate and later mounted in Entellan (Sigma-Aldrich). Lignin
228 was detected with 0.5% Safranin-O (Acros organics) in an aqueous solution; stained for 20
229 seconds followed by three washes in water. Slides were mounted in Entellan (Sigma-Aldrich)
230 after drying. Imaging was done using a Zeiss AxioImager microscope.

231

232 **2.7 Immunolabelling**

233 Seeds at 10, 14, and 18 DAP from CT and HT, in two biological replicates, were fixed in 4% w/v
234 paraformaldehyde in ice-cold PEM buffer (50 mM PIPES, 5 mM EGTA, and 5 mM $MgSO_4$, pH
235 6.9). Samples were incubated on ice under vacuum for twice 1 h with fresh fixative solution,
236 followed by overnight incubation at 4°C. The samples were washed twice with ice-cold PEM
237 buffer, dehydrated through an ethanol series (50%, 70%, 80%, 90% and 100% three times)
238 under vacuum and infiltered with increasing concentrations (30%, 50% and 100%) of LR white
239 resin (Agar Scientific) in absolute ethanol over 8 days before being polymerised at 60°C for 24
240 h. Six seeds by timepoint per growth condition per biological replicate were sectioned (1 µm
241 thickness) using a glass knife mounted on a Leica RM2265 or EM UC7 microtome.
242 Immunolocalizations were performed with JIM5, LM19, LM20, and LM25 antibodies
243 (Agrisera). For immunolocalisation with LM25, an incubation with 0.1% pectolyase in 1X PBS
244 was done for 25 min at room temperature and washed once in 1X PBS before the blocking
245 step. For immunolocalisation with JIM5, LM19, and LM25, the sections were blocked with 3%
246 w/v BSA in 1X PBS and incubated for 1 h at room temperature. For the immunolocalisation
247 with LM20, an incubation in CAPS buffer (50 mM CAPS and 2 mM $CaCl_2$) for 1 h followed by
248 three washes with 1x PBS was performed before blocking with 3% skimmed milk in 1X PBS.
249 Sections were incubated with 1:10 v/v dilution of antibody prepared with 1% BSA in 1X PBS
250 for JIM5, LM19 and LM25 and 1% skimmed milk in 1X PBS for LM20 overnight at 4°C in a
251 humid chamber. The sections were brought to room temperature for 1 h, washed three times
252 with the above-mentioned buffers and incubated for 1 h in a humid chamber in the dark with
253 the secondary antibodies. A dilution of 1:100 v/v of secondary antibodies [anti-rat IgG Alexa

254 488 (Thermo Fisher) or anti-rat IgG Dylight 488 (Agrisera) for JIM5 and anti-rat IgM Dylight
255 488 (Thermo Fisher) for LM19, LM20 and LM25] in 1% BSA or 1% skimmed milk in 1X PBS was
256 used. Sections were washed in the respective buffers and 1X PBS, counterstained with 0.025
257 mg/ml Calcofluor white (Sigma-Aldrich), and mounted with VECTASHIELD antifade mounting
258 medium (Eurobio). The images were obtained with the ZEISS Axioimager 2 with a 40X dry
259 objective.
260 The intensity of the immunofluorescence in the cell walls of the epidermal and palisade layers
261 of the seed coat was quantified using ImageJ software. Images were adjusted using min/max
262 settings for optimal representation of fluorescent signals. For the three epidermal layers, a
263 segmented line with a width of 25 points was used to manually mark the cell walls of adjacent
264 cells of the same layer. The sum of fluorescence intensity in the three epidermal layers was
265 represented as one measurement. A region of interest was marked using the polygon
266 selection tool for the palisade layer. The mean fluorescence value obtained over the marked
267 regions for the different layers was subtracted from the background signal over the same area
268 to obtain the final fluorescence intensity.
269
270 **2.8 Cell wall profiling from the seed coat**
271 The enzymatic fingerprinting of the cell wall of seed coat from 10, 14 and 18 DAP seeds grown
272 under CT and HT conditions was performed in three biological replicates. The seed coats were
273 dissected from the seeds and were submerged in 96% (v/v) ethanol. The ethanol fraction was
274 discarded, and the seed coats were dried in a speed vacuum concentrator at 30°C overnight.
275 Dried seed coats were digested with 5 U/mg DW sample of *Pectobacterium carotovorum*
276 endo-polygalacturonase or *Paenibacillus* sp. xyloglucanase (Megazyme, Bray, Ireland) in 50
277 mM ammonium acetate buffer (pH 5) at 37°C for 18 h. Samples were centrifuged at 13,000
278 rpm for 10 min, and 100 µl of the supernatants were transferred into vials. For MS analysis,
279 10 µl of each fraction was injected. The oligosaccharides released from digestion were
280 separated according to Voxeur et al. (2019). Xyloglucan and pectin fragments were analysed
281 using an HPLC system (UltiMate 3000 RS HPLC system, Thermo Scientific, Waltham, MA, USA)
282 coupled to an Impact II Ultra-High Resolution Qq-Time-Of-Flight (UHR-QqTOF) spectrometer
283 (Bruker Daltonics, Bremen, Germany) equipped with an electrospray ionisation (ESI) source
284 in negative mode with the end plate offset set voltage to 500 V, capillary voltage to 4000 V,
285 nebuliser to 40 psi, dry gas to 8 l/min and dry temperature of 180°C. The Compass 1.8

286 software (Bruker Daltonics) was used to acquire the data. Chromatographic separation was
287 performed on an ACQUITY UPLC Protein BEH SEC Column (125A, 1.7 µm, 4.6 mm X 300 mm,
288 Waters Corporation, Milford, MA, USA) coupled with guard Column BEH SEC Column (125A,
289 1.7 µm, 4.6 mm X 30 mm). Elution was performed in 50 mM ammonium formate and 0.1%
290 formic acid at a flow rate of 0.4 ml/min and with a column oven temperature of 40°C.
291
292 **2.9 Space-restricted growth of siliques**
293 Silicone tubes with 3-mm cross-section were inserted over developing siliques at 10 DAP and
294 12 DAP under HT and CT conditions, respectively, in four biological replicates with roughly 20
295 siliques per replicate. A 10 DAP silique at HT has a similar silique thickness to a 12 DAP silique
296 at CT. Siliques from the same growth conditions without a silicone tube were used as negative
297 control. The number of total, intact, dead and SCR seeds per siliques were estimated when
298 mature and fully dry. For seed coat thickness measurements of space restricted seeds, seed
299 embedding with LR white and seed sectioning (protocol described in section 2.7) was used
300 followed by toluidine blue staining (protocol described in section 2.5). For seed coat thickness
301 measurements, and seed and embryo size measurements, seeds at 24 DAP from CT and 20
302 DAP from HT were used which are at the same developmental stage.
303
304 **2.10 Nanoindentation**
305 A cylindrical 3D-printed mould of 2-cm diameter and 0.5-cm height was created with multiple
306 circular wells of 1.8 to 2.4 mm diameter and 1.5-mm depth on the surface for holding the
307 Topas seeds in place during the measurements (Fig. S7). Three 24 DAP seeds from CT and
308 three 20 DAP seeds from HT conditions were used for this study. A Hysitron TI 950 instrument
309 (upgraded to TI980) equipped with a diamond conical indenter with a cone angle of 90° and
310 a tip radius of 0.97 µm was used for the nanoindentation. The indenter was calibrated on
311 fused silica standard and tested on polycarbonate standard sample. Accelerated mechanical
312 property mapping (XPM) was applied, as this mode enables the acquisition of elastic modulus
313 maps with high spatial resolution and short acquisition times. Compared to the classical
314 quasistatic indentation method, XPM is substantially faster, the time required to perform a
315 single quasistatic indent is more than one order of magnitude longer. The reduced
316 measurement time minimizes the effects of thermal drift, seed drying and suppresses the
317 time-dependent mechanical response of the seed material. The maximum load was set to 50

318 µN, with a loading time of 0.5 s, a holding segment at the maximum load of 0.5 s, and an
319 unloading time of 0.1 s. Each measurement consisted of a 7 × 7 array of indents covering an
320 area of 7 × 7 µm². In total, more than 150 nanoindentation data points were acquired using
321 this method. The data were evaluated according to (Oliver & Pharr, 1992). The indentation
322 reduced modulus values were acquired directly from the analysis of the indentation unloading
323 curves. The reduced modulus E_r is calculated as a combination of the sample material and
324 indenter elastic deformations:

325 $$\frac{1}{E_r} = \left(\frac{1-\nu_i^2}{E_i}\right) + \left(\frac{1-\nu_s^2}{E_s}\right)$$

326 Here, E_s, ν_s and E_i, ν_i are the Young moduli and Poisson ratio values of samples and the
327 diamond indenter, respectively. If the studied samples exhibit low elastic moduli compared
328 to diamond, the first term in equation may be neglected.
329

330 **2.11 Statistical analysis**

331 GraphPad Prism v.8.4.3 was used to plot the graphs and calculate the statistical significance
332 using either ANOVA or multiple comparison tests. For the RNA sequencing experiment, R
333 programming was used to analyse and represent data and obtain the statistical significance.
334

335 **3. RESULTS**

336 **3.1 *Brassica napus* seed coat integrity is affected by long-term heat stress**

337 We have previously reported that in *Brassica napus* cv. Topas the early seed development is
338 affected under long-term heat treatment (HT) (Mácová et al., 2022). This study focuses on
339 the seed coat rupture (SCR) observed in seeds of Topas developed under HT (Fig. 1b), starting
340 at 20 DAP, while this phenomenon has very rarely been observed in seeds grown under
341 control treatment (CT) (Fig. 1a, Fig. S1). The SCR phenotype occurred with variable outcomes,
342 from a minor or incomplete testa break with intact tegmen and embryo remaining within the
343 seed to a complete seed coat rupture resulting in the embryo root or shoot protruding
344 through the break site appearing like a germinated seed (Fig. 1b, Fig. S1d-g). Such embryos
345 often had distinguishable phenotypes (Fig. S1g). The quantification of the seed phenotypes
346 by counting number of dry seeds per silique revealed a significant decrease in percent of
347 intact seeds, accompanied by a significant increase in the proportion of dead seeds and SCR

seeds for plants developed under HT compared to that of CT (Fig. S1h). At HT, approximately 50% of the seeds in a silique underwent SCR (Fig. 1c).

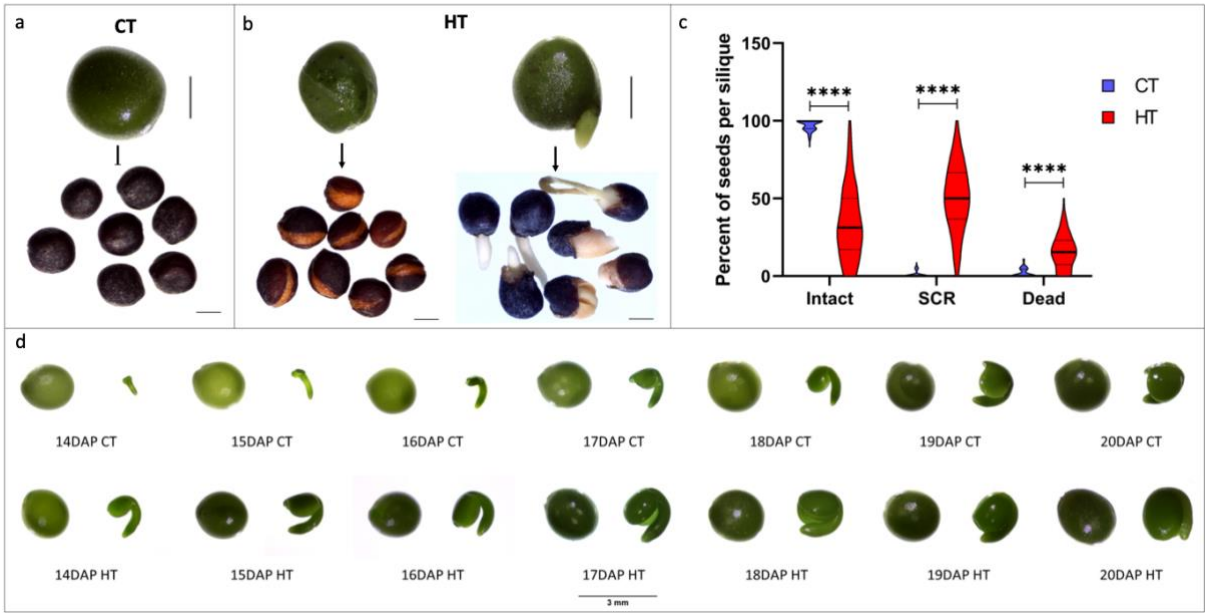

Fig. 1. SCR phenotype observed in Topas seeds developed under HT. (a) 26 DAP seeds and matured dry seeds after harvest grown under CT. (b) 26 DAP seeds and matured dry seeds after harvest grown under HT depicting the seed coat rupture (SCR); on the left are seeds with incomplete testa rupture and on the right, seeds with fully ruptured seed coat with protruding embryos. (c) Quantification of the percentage of dry seeds per silique from CT (blue) and HT (red) showing the percent of intact, SCR and dead seeds (n CT= 116, n HT= 245). Phenotypic classification represented in Fig. S1a-c. Asterisks indicate statistically significant differences in HT in a multiple t-test using the Holm-Sidak method (**** corresponds to *p*-values of $p < 0.0001$. (d) Embryo stage of seeds developed on CT (top) and HT (bottom) from 14 to 20 DAP. The isolated embryo shown on the right is from the seed on the left. Scale bars: 1 mm (a,b) and 3mm (d).

3.2 The embryo-to-seed size ratio is increased at HT

Embryo staging of the seeds from 14 to 20 DAP revealed that embryo development is accelerated in seeds developed under HT compared to seeds grown under CT (Fig. 1d), which is consistent with our previous observations in seeds at early developmental stages (Mácová et al., 2022). We estimated that the embryos in the seeds at HT were four days ahead of the embryos in seeds at CT in their developmental stage, e.g., a 14 DAP embryo at HT would be developmentally similar to an 18 DAP embryo at CT (Fig. 1d).

370 We studied the seed area and embryo area of seeds at 14 DAP to 20 DAP at CT and HT.
371 Embryos at HT were more than twice the size of those at the same DAP at CT (Fig. 2a). The
372 seed area increased from 14 to 20 DAP, and this increase was reduced from 20 DAP as the
373 seeds entered the maturation phase (Fig. 2b). The seed size at 18 DAP was significantly larger
374 under HT than under CT (Fig. 2b). We noticed that the seeds did not undergo a compensatory
375 increase in size to accommodate the HT-induced larger embryos. The embryo-to-seed area
376 ratio provides valuable insight into the space occupied by the embryo within the seed at a
377 given DAP under the two growth conditions (Fig. 2c). We observed that the embryos
378 developed under HT filled significantly more space in the seed than those grown under CT.
379 These observations suggest that the accelerated embryo growth in HT resulted in the
380 formation of larger embryos but not larger seeds. When the seed and embryo size were
381 compared accounting the same embryo developmental stage; at HT, 14 DAP seed and embryo
382 size were smaller compared to 18 DAP seeds from CT.
383 As the embryonic developmental shift could be observed phenotypically, we investigated the
384 transcript profiles by RNA-seq of these seeds (14, 18, 20 DAP) developed in CT and HT. A
385 Principal Component Analysis (PCA) maps sample relationships (Fig. S2). The 14 DAP seeds
386 from HT clustered together with the 18 and 20 DAP seed samples from CT, further validating
387 the observations of the HT-induced accelerated seed developmental process. Next, we
388 screened the gene ontology (GO) enrichment analysis for GO terms associated with the
389 process of seed development and cell cycle regulation (Fig. 2d, Fig S3). A significant
390 enrichment of GO terms associated with seed maturation and positive regulation of
391 transcription was found when comparing the HT and CT datasets from seeds of the same age
392 or same development stage: 14 DAP HT vs. 14 DAP CT, 18 DAP HT vs. 18 DAP CT, and 14 DAP
393 HT vs. 18 DAP CT. GO terms associated to DNA biosynthesis, replication and mitotic DNA
394 replication initiation are significantly enriched comparing the datasets from SCR and non-SCR
395 20 DAP seeds developed at HT (Fig. S3).

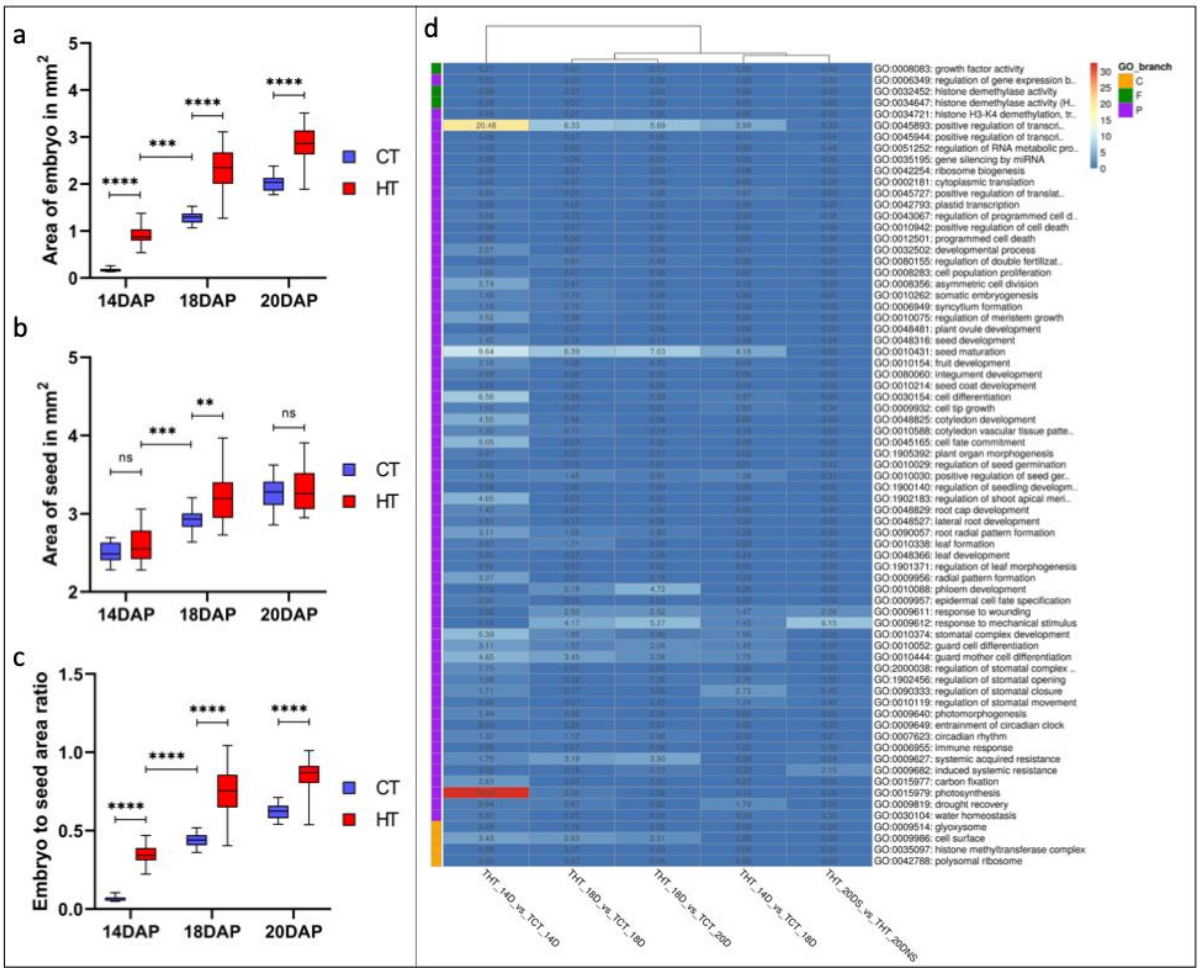

Fig. 2. Embryo and seed size measurements of *Brassica napus* cv. Topas seeds developed at CT and HT. (a, b) Embryo (a) and seed (b) area measurements in mm^2 of 14, 18 and 20 DAP Topas seeds developed at CT (blue) and HT (red). (c) Ratio of embryo-to-seed size 14, 18 and 20 DAP Topas seeds developed at CT and HT. Asterisks indicate statistically significant differences in HT and between 14 DAP HT and 18 DAP CT in a two-way ANOVA test with Sidak's multiple comparisons (*, **, *** and **** correspond to *p*-values of $0.05 > p > 0.005$, $0.005 > p > 0.0005$, $0.0005 > p > 0.0005$ and $p < 0.00005$, respectively); n.s., not significant. (d) Upregulated GO terms ($Log_2FC \geq 1.32$) related to plant development with the transcriptional response of Topas seeds to HT (values in the box depict $-log_{10}$q-value).

3.3 The formation of larger embryos at HT impacts the thickness of the seed coat cells

We hypothesised that the accelerated embryo growth and the possible early transition into the seed maturation phase may interfere with the maternally-derived seed coat development, thereby inducing the SCR phenotype. The seed coat of *B. napus* is composed of three layers of cells (Fig. 3a): an outer epidermal layer of three cell files, a middle palisade

412 layer made of a single layer of cells with substantial secondary cell walls, and an inner
413 endothelial layer surrounding the endosperm (Jiang & Deyholos, 2010). The thickness of these
414 three layers of the seed coat was measured in seeds of 10, 14, 18, 20, and 22 DAP developed
415 under CT and HT (Fig. 3). Seed coat thickness was not affected by HT in 10 DAP seeds (Fig. 3f-
416 h). However, all three seed coat layers were significantly thinner in older seeds developed
417 under HT (Fig. 3b-h). Taking into account of the same developmental stage of the embryo, we
418 compared the seed coat thickness of seeds from 18 DAP at CT and 14 DAP at HT and observed
419 a significant reduction in thickness of the three layers (Fig. 3b-e). The palisade and the first
420 endothelial layers were the most affected by this reduction, with a 46% reduction in
421 endothelial cell layer thickness induced by HT as the seed aged from 14 DAP to 20 DAP,
422 whereas the thickness reduction was only 12% at CT (Fig. 3i). These results indicate that the
423 HT-induced accelerated embryo growth between 14 and 20 DAP could have physical effects
424 on the development of maternally-derived seed coat cells leading to the thinning of seed coat
425 layers. At equivalent stages of development in Arabidopsis, the seed coat cells are thought to
426 stop dividing, and seed size expansion would rely on seed coat cell elongation (Figueiredo et
427 al., 2016; Garcia et al., 2005; Haughn & Chaudhury, 2005). We hypothesised that faster
428 embryonic growth might result in strain building up among the seed coat cells, promoting cell
429 elongation and providing space for the embryo to expand. In this context, we performed a
430 detailed examination of cell wall constituents in the seed coat.

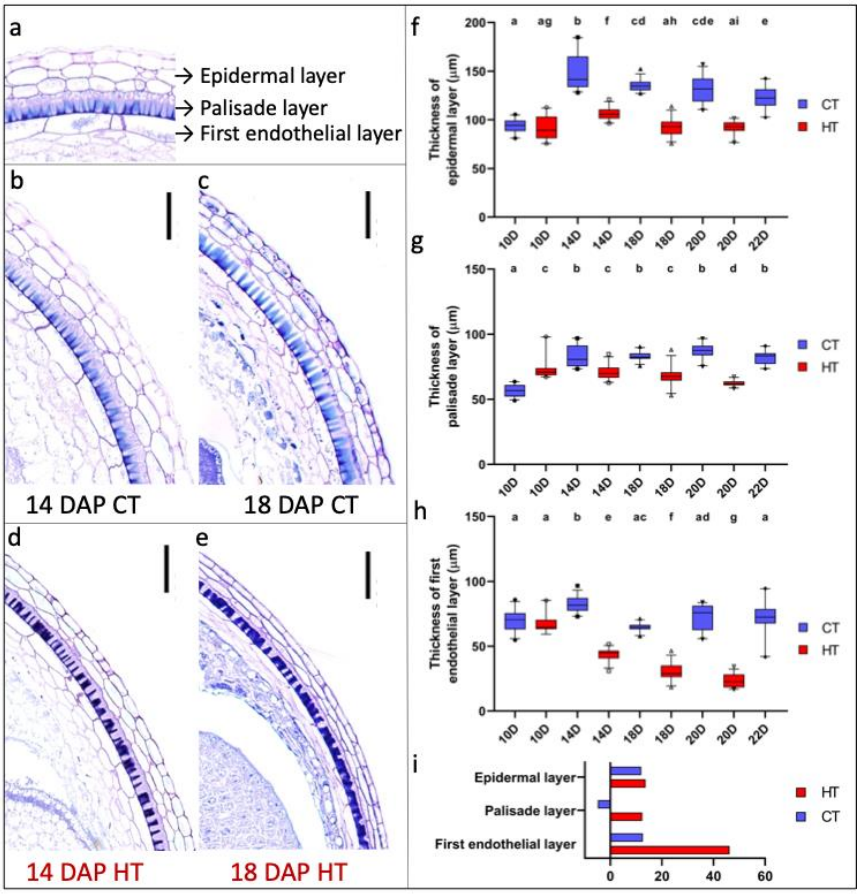

Fig 3. The thickness of the seed coat cells is reduced in HT. (a-e) Histological sections of Topas seeds focused on the seed coat, stained with toluidine blue. (a) The seed coat is composed of an epidermal layer, a palisade layer and an endodermal layer. (b-e) Seed coat of 14 DAP seeds from CT (b) and HT (d) and 18 DAP seeds from CT (c) and HT (e). Scale bars represent 200 µm. (f-h) Box-whisker plots show the size mean, median, outliers, and SD in µm of the thickness of the epidermal layer (f), palisade layer (g) and first endothelial cell layer (h) in 10, 14, 18, and 20 DAP seeds from CT (blue) and HT (red). Samples with the same letter were not statistically significantly different. (i) Percentage of reduction in thickness as the seed aged from 14 to 20 DAP.

3.4 The composition and properties of the seed coat cell wall are altered in HT-grown seeds

Given the developmental differences between CT and HT, we compared the RNA-seq datasets based on the embryo morphology, rather than seed age: 18 DAP (TCT_18D) versus 14 DAP (THT_14D). We also compared the transcriptome profiles of seeds exhibiting SCR (THT_20DS) and non-SCR (THT_20DNS) phenotypes. GO enrichment analysis revealed significant differences in the regulation of many pathways related to plant cell walls (Fig. 4a). These

448 included GO terms related to cell wall biogenesis, cell wall thickening, and cell wall
449 modification. Interestingly, the datasets of HT-grown seeds also showed overrepresentation
450 of cellulose, pectin, and xyloglucan metabolism and modification pathways, including the
451 pectinesterase, pectinesterase inhibitor and pectin catabolic pathways. Examining the
452 differentially expressed genes (DEGs) associated with pectin metabolic pathways revealed
453 differential regulation of enzymes such as galacturonosyltransferases (GAUTs), which are
454 involved in pectin biosynthesis (Mohnen, 2008), pectinesterases and pectinesterase
455 inhibitors, involved in the chemical modification of pectin (Wormit & Usadel, 2018; Wu et al.,
456 2018; Xu et al., 2022), and polygalacturonases and pectate lyases, which are involved in pectin
457 degradation (Marin-Rodriguez, 2002; Park et al., 2010; Safran et al., 2023) (Fig. 4b). This
458 suggests that heat stress may regulate the chemical modification of pectin, a major cell wall
459 constituent.
460 To confirm whether transcriptional changes in cell wall-modifying enzymes affect the
461 secondary cell wall, the levels of pectin and lignin in the seed coat of HT-grown seeds were
462 tested using Ruthenium Red (Fig. 4c), which stains red the polyanionic molecules in the
463 deesterified pectin monomers (Nagayama et al., 2019), and Safranin-O (Fig. S4), which stains
464 the phenolic lignin compounds in bright red (Bond et al., 2008). The cells of the palisade layer
465 in the seed coat of 14 and 18 DAP Topas seeds grown under HT were stained red more
466 intensively by both dyes than in the 14, 18 and 22 DAP seeds grown under CT. These
467 observations suggest that, as they enter the maturation phase, seeds accumulate more
468 secondary cell wall elements in the seed coat under HT conditions than under CT conditions.

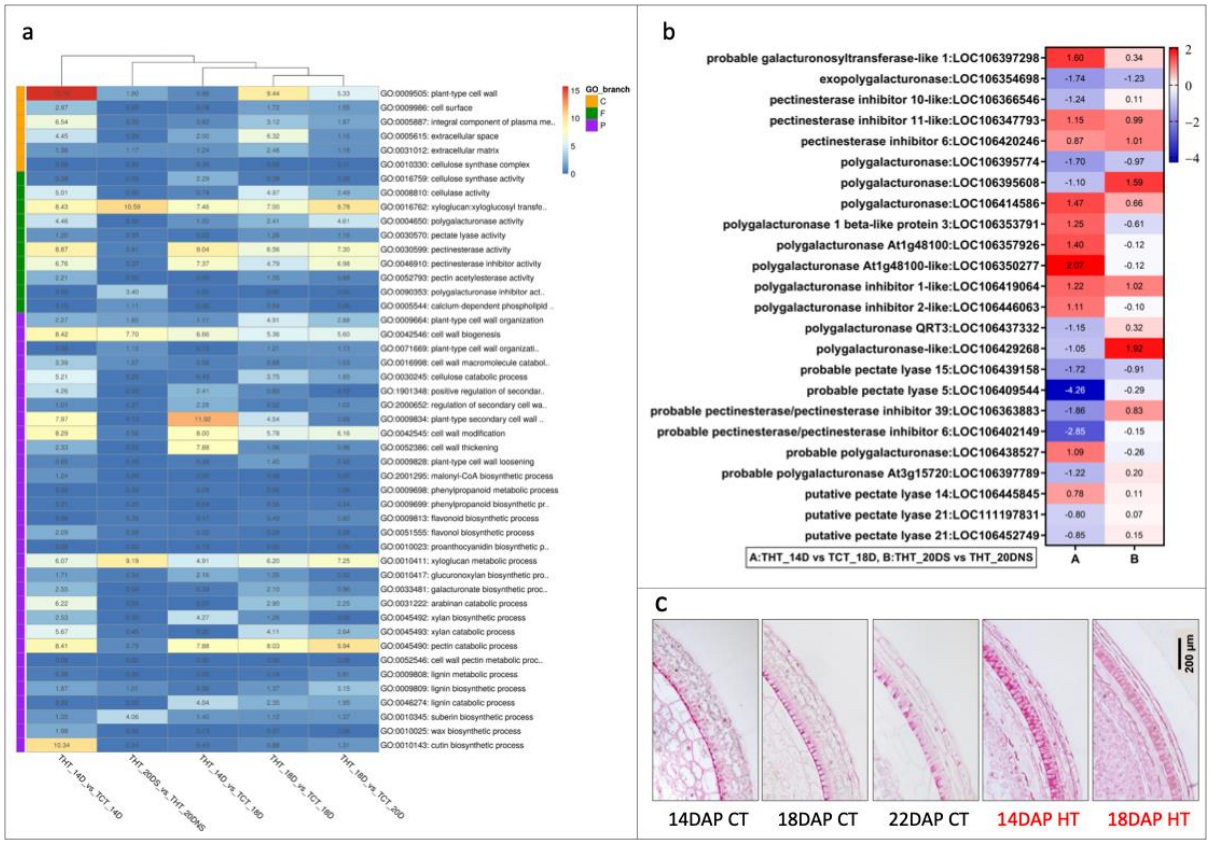

Fig. 4. Transcriptional changes in Topas seeds associated with growth at HT indicate changes in cell wall composition. (a) GO terms associated to cell wall metabolism and regulation with the transcriptional response of Topas seeds to HT are shown (values in the box depict $-\log_{10}$q-value). (b) Heatmap showing the differential transcription of selected genes involved in pectin metabolism in 14 DAP HT vs 18 DAP CT seeds (A), and SCR vs non-SCR seeds (B) at 20 DAP from HT. The full dataset is presented in Tables S1 and S2. (c) Histological sections of Topas seeds focused on the seed coat, stained with Ruthenium Red for pectin. Sections of 14, 18, and 22 DAP CT seeds and 14 and 18 DAP HT seeds are shown. Scale bars represent 200 µm.

3.5 HT accelerates the process of demethylesterification of pectin in the cell wall of the seed coat

We further investigated the presence of pectin and hemicellulose in the layers of the seed coat by immunostaining with selective antibodies (Fig. 5a-c, Fig. S5a). To detect pectin, which is primarily composed of homogalacturonan (HG), we used the LM19 antibody, which binds preferentially to demethylesterified HG, the LM20 antibody that binds preferentially to methylesterified HG, and the JIM5 antibody, which exhibits a high affinity for partially demethylesterified HG (Fig. 5a-c). For hemicellulose, mainly composed of xyloglucan, we used

487 the LM25 antibody (Fig. S5a). The seed coat of 14 and 18 DAP HT-developed seeds had
488 significantly higher fluorescence levels of the LM19 and JIM5 antibody signals in the palisade
489 layer, indicating an increase in demethylesterified HG in HT seeds (Fig. 5a,b). In contrast, no
490 significant differences in fluorescence intensity for the LM20 antibody signal were observed
491 in the palisade layer in the seed coat of CT and HT seeds (Fig. 5c). In the epidermal layer of
492 HT-developed seeds, the JIM5 and LM19 antibody signal was significantly higher from 14 DAP
493 seeds, while this increase happens at 18 DAP in CT seeds (Fig. 5a,b). The LM20 antibody signal
494 was significantly lower in 18 DAP HT seeds than in all other samples, indicating a reduction in
495 the amount of methylesterified HG (Fig. 5c). These results suggest an early enrichment of
496 pectin and a shift towards demethylesterified pectin in the cell walls of the palisade and
497 epidermal cells in 14 DAP HT-grown seeds. LM25 fluorescence was significantly higher only in
498 the palisade cells of 18 DAP HT-grown seeds compared to CT seeds, suggesting a slight effect
499 of temperature on the amount of xyloglucan in the seed coat of these seeds (Fig. S5a).

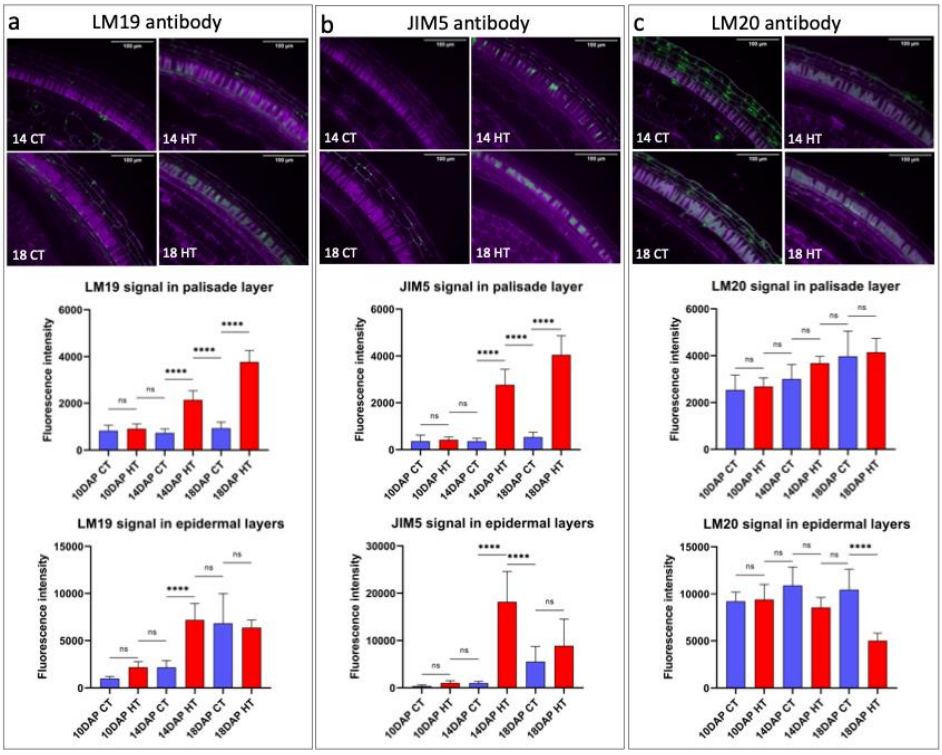

500

501 **Fig. 5** Immunolocalization to estimate the degree of pectin methylation using LM19, JIM5,
502 and LM20 antibodies on the seed coat of 14 and 18 DAP CT and HT seeds. The signal is visible
503 in green; the cell structure is marked in magenta with calcofluor white. Scale bars represent
504 100 µm. Fluorescence intensity was measured in epidermal and palisade cells in 10, 14 and
505 18 DAP HT and CT seeds. Asterisks indicate statistically significant differences in HT and

506 between seed ages in a one-way ANOVA test with Tukey multiple comparisons (*, **, *** and
507 **** correspond to *p*-values of 0.05 > *p* > 0.01, 0.01 > *p* > 0.001, 0.001 > *p* > 0.0001 and *p* <
508 0.0001, respectively); n.s., not significant.
509
510 To confirm our microscopic observations, we performed enzymatic fingerprinting of the cell
511 wall of the isolated seed coats from 10, 14 and 18 DAP seeds of Topas grown at CT and HT
512 (Fig. 6a). Digestion of HG by an endo-polygalacturonase between demethylesterified ester
513 stretches of the galacturonic acid (GalA) releases several oligogalacturonans (OGs). OGs have
514 been termed GalAxMeyAcz based on the degree of polymerisation of GalA and the number
515 of methyl and acetyl groups. In our analysis of the Topas seed coat, we identified GalA3,
516 GalA3ox, GalA3Xyl, GalA3Me, GalA3MeAc, GalA4Ac, GalA4Me, GalA4Meox, GalA4Me-H_2O,
517 and DPx>4Mey (methylesterified OGs with degree of polymerisation greater than 4). The total
518 peak area obtained from the MS analysis was plotted by grouping OGs with and without
519 methyl groups (Fig. 6b). A significant increase of demethylesterified OGs was released from
520 the cell walls of 14 DAP seed coat at HT compared to CT, which correlates with the signal
521 intensity of the LM19 antibody binding to the demethylesterified HGs in the cell walls in the
522 seed coat layers (Fig. 6b,c). Similarly, a significant increase in the methylesterified OGs with
523 varying numbers of methyl groups in the seed coats of 14 DAP correlates with the signal
524 intensity of JIM5 antibody binding to partially methylesterified HGs in the cell walls of the
525 epidermal and palisade layers (Fig. 6b,c). The release of oxidised OGs is also notable, as this
526 may reflect the presence of long oxidised OGs trapped within the pectin and not solubilised
527 through alcohol extraction. Regarding xyloglucan, LXXGAc levels remained unchanged and
528 correlated with the LM25 signal in the seed coat (Fig. S5b,c). However, a significant increase
529 in the level of fucosylated subunits was observed in the 14 DAP seed coats of HT compared
530 to CT (Fig. S5b).
531 Using a variety of approaches, we uncovered that, between 14 and 18 DAP, seeds grew more
532 at HT than at CT, probably due to the pressure exerted by embryo growth. We also found that
533 growth at HT altered the properties of the cell walls in the seed coat of seeds from 14 DAP
534 onwards. The cell walls of the epidermal and palisade cells accumulated more pectin and
535 shifted prematurely towards producing demethylesterified pectin, which may have prevented
536 the cells from elongating. Consequently, seeds grown at HT stopped to grow after 18 DAP, as
537 the changes to the cell walls stiffened them and inhibited seed growth.

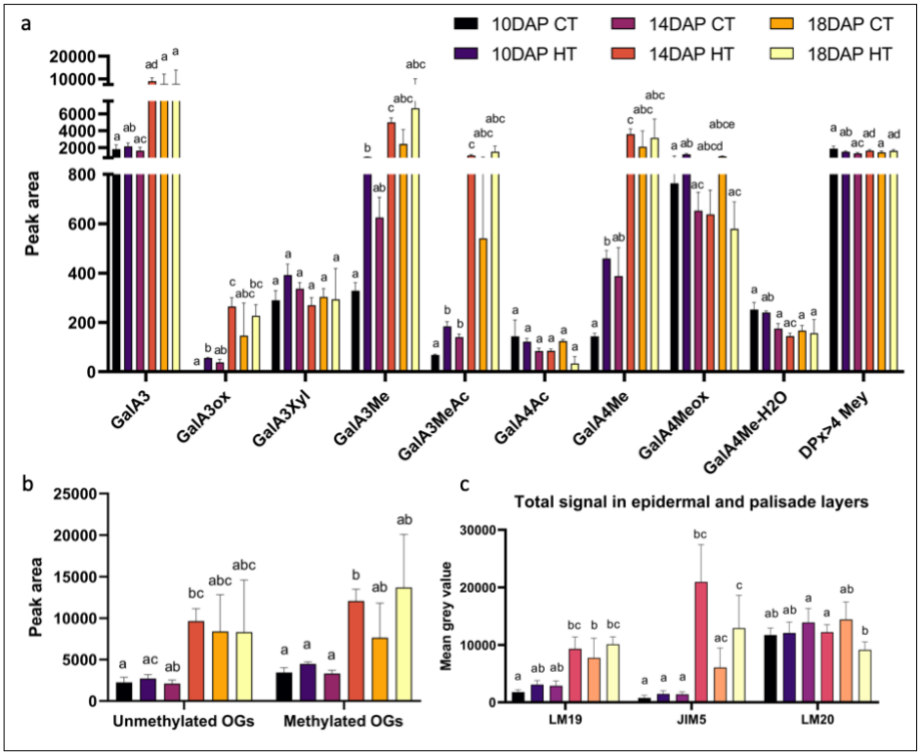

Fig. 6 Pectin enzymatic profiling. (a) Pectin composition of the seed coat cell wall of 10, 14, and 18 DAP seeds from HT and CT. The graph shows the measurements expressed as peak area from the MS analysis for GalA3, GalA3ox, GalA3Xyl, GalA3Me, GalA3MeAc, GalA4Ac, GalA4Me, GalA4Meox, GalA4Me-H_2O and DPx>4Mey (methylesterified OGs with degree of polymerisation greater than 4). (b) Graph showing the amount grouped as methylesterified versus non-methylesterified OGs from (c) Graph showing the total intensity signal for pectin from (Fig. 5).

3.6 HT affects the physical properties of the seed coat

The composition of the seed coat cell wall determines its mechanical strength (Mendu et al., 2011; Sechet et al., 2018). The enrichment of GO terms associated with secondary cell wall metabolism and the high content of demethylesterified pectin in the seed coat prompted us to investigate whether growth at a high temperature affects the mechanical strength of *B. napus* seed coat cell walls. We hypothesised that the increased demethylesterified pectin accumulation not only makes the wall stiffer and less extensible, but also makes it more prone to rupture, causing SCR. We analysed the mechanical properties of the seed coat cell wall using a nanoindentation technique, which provided valuable insights into the elastic modulus E_r (MPa). Elastic modulus quantified the elastic response of the seed surface, e.g., its ability

557 to return to its original shape after the release of the mechanical stress. It indicates how much
558 a material deforms temporarily (elastically) (Lapointe et al., 2025). It is a measure of stiffness,
559 meaning the resistance of the seed to elastic deformation. In this study, we compared seeds
560 at 20 DAP from HT and 24 DAP from CT, to ensure that seeds at the same embryo
561 developmental stage were analysed. HT seeds were found to have a significantly lower elastic
562 modulus than CT seeds (Fig. 7a). It indicates that the seed coat of CT seeds can withstand
563 higher mechanical stress during elastic deformation than the seed coat of HT seeds, suggesting
564 that HT seeds are stiffer.

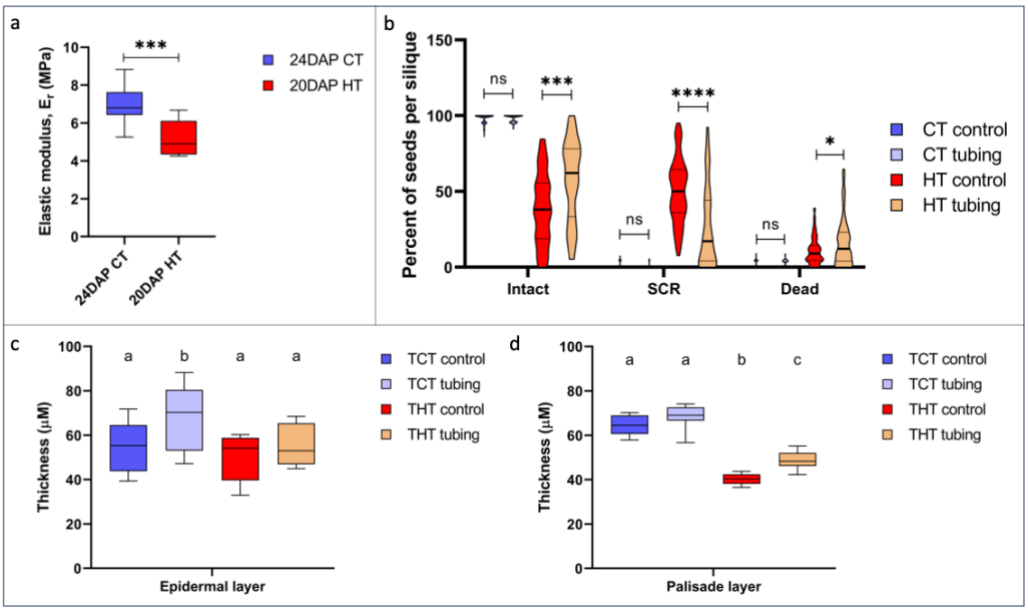

565

566 **Fig. 7** Seed coat mechanobiology of *B. napus* seeds. (a) Measurement of elastic modulus, E_r
567 (MPa), comparing 20 and 24 DAP seeds from CT and HT respectively. (b) A 3-mm silicon tube
568 was applied to siliques from 10 DAP CT and 12 DAP HT. Dry seeds were quantified for the
569 percent of intact, SCR and dead seeds per silique. Asterisks indicate statistically significant
570 differences in HT and between seed ages in a two-way ANOVA test with Tukey multiple
571 comparisons (*, **, *** and **** correspond to *p*-values of 0.05 > *p* > 0.01, 0.01 > *p* > 0.001,
572 and *p* < 0.001, respectively); n.s., not significant. (d,e) Box-whisker plots show the size,
573 median, outliers, and SD in µm of the thickness of the epidermal layer (c), palisade layer (d)
574 of seeds at 24 DAP from CT and 20 DAP from HT to account for same developmental stage.

575

576 **3.7 Application of mechanical constraints during silique development partially rescues SCR**
577 **phenotype**

578 We demonstrated that the seed coat of seeds developed under HT conditions exhibited
579 reduced elastic stiffness and hardness. We then hypothesised that such a seed coat would
580 lack the mechanical strength required to withstand the mechanical stress imposed by the
581 faster-developing embryo, resulting in SCR. Should this be the case, then providing external
582 support to oppose continuous embryo growth would prevent the seeds from the occurrence
583 of SCR. To test this hypothesis, we encased the developing siliques in a silicone tube to create
584 an external mechanical constraint for the seeds, in an attempt to counteract the pressure
585 exerted by the developing embryo on the seed coat (Fig. S6a). It has been demonstrated that
586 applying a mechanical force to the siliques triggers seed maturation by arresting embryonic
587 growth in *B. napus* Reston cv. (Rolletschek et al., 2024). In the CT and HT seeds encased by
588 silicone tube, the embryo size was significantly reduced indicating that the space restriction
589 has constrained the growth of the embryo whereas the ratio of embryo to seed area remained
590 same (Fig. S6c-e). The presence of the silicone tube on the siliques of CT plants did not affect
591 seed viability or promote SCR (Fig. 7b, S6b). Under HT conditions, the external support
592 provided by the silicone tube on the siliques resulted in a significant decrease in the number
593 of seeds undergoing SCR and an increase in the number of intact seeds (Fig. 7b, S6b).
594 Measuring the thickness of the seed coat layers of HT-grown seeds revealed that the palisade
595 layer thickness increased significantly in seeds encased by the silicone tube compared to
596 seeds developed in uncased siliques (Fig. 7c,d). This external mechanical support reinforced
597 the compromised mechanical strength of the seed coat caused by faster embryo
598 development.
599
600 **4. DISCUSSION**
601 Rising global temperatures have an adverse effect on the production of major staple crops
602 (Agnolucci et al., 2020; Jägermeyr et al., 2021) by hindering the development of seeds, as we
603 observed in *Brassica napus* (Mácová et al., 2022). Understanding how plants perceive heat
604 stress during seed development provides valuable insights into breeding temperature-
605 resilient crops which is of great importance in a changing climate. In our previous study, the
606 occurrence of temperature-induced *in vivo* sprouting was reported in three spring cultivars of
607 *B. napus* (Mácová et al., 2022), which affected seed viability and oil quality. Prolonged growth
608 of Topas at high temperatures resulted in half of the seeds per silique undergoing SCR, a
609 phenomenon rarely observed under optimal conditions. In this study, we aimed to

610 understand the process resulting in the high-temperature-induced SCR phenotype in *B. napus*
611 Topas cv. during late seed development focusing on seed coat development, cell wall
612 modifications and biomechanics.
613 The integration of signalling pathways and the physical interactions between the three tissues
614 that comprise the seed - the seed coat, the endosperm, and the embryo - determine the final
615 size, shape, and dormancy state of the mature seed (Li et al., 2019). The *Arabidopsis iku2-2*
616 *zou-4* double mutant exhibits reduced seed viability due to developing seeds undergoing testa
617 rupture (Creff et al., 2015), a phenomenon analogous to the SCR phenotype observed in Topas
618 seeds developed at HT. The *haiku2 (iku2)* mutation leads to elevated endosperm pressure,
619 triggering mechanosensitive premature stiffening of the testa. This is likely associated with
620 the accumulation of demethylesterified pectin, ultimately resulting in smaller *iku2* seeds
621 (Creff et al., 2023). Seeds of *zhoupi-4 (zou-4)* have a persistent endosperm at the torpedo
622 stage, even as the embryo expands in size, resulting in large seeds. Testa rupture in *iku2-2*
623 *zou-4* seeds may be a consequence of early stiffening of the testa together with increased
624 pressure from the developing embryo and a persistent endosperm. We hypothesise that a
625 similar process occurs in *B. napus* cv. Topas seeds, whereby high temperature alters the
626 mechanosensing-dependent interaction between the embryo and the testa. From the earliest
627 stages onward, high temperature accelerated embryogenesis, resulting in an approximately
628 four-day developmental advancement by the onset of seed maturation (Mácová et al., 2022)
629 and this study). Although final seed size was not affected, the enlarged embryos occupied
630 most of the space in the seed cavity, thereby increasing mechanical stress on the surrounding
631 seed coat and generating tension between the cells involved in seed size regulation. In
632 Arabidopsis, the endosperm plays a significant role in modulating seed coat properties and
633 determining seed size. Owing to technical limitations in *B. napus* Topas seeds, we were unable
634 to assess whether high temperature similarly affected the endosperm. At comparable
635 developmental stages in Arabidopsis, seed size is primarily determined by seed coat cell
636 elongation rather than cell division (Figueiredo et al., 2016; Garcia et al., 2005; Haughn &
637 Chaudhury, 2005). The reduced thickness of the epidermal, palisade and endothelial layers of
638 the seed coat observed in high temperature-developed Topas seeds suggests that these cells
639 accommodated increased mechanical tension predominantly through cell stretching rather
640 than proliferation. To withstand the strain generated between adjacent seed coat cells and

641 the pressure exerted by the expanding embryo, compensatory stiffening of the seed coat cell
642 wall likely occurred.
643 The extensibility of the seed coat cells is determined by cell wall composition and the
644 interactions among its structural components, which together permit embryo expansion.
645 Transcriptomic analysis of the seeds revealed temperature-dependent differential regulation
646 of cell wall-related pathways, with enrichment of genes associated with cellulose, pectin and
647 xyloglucan metabolism, secondary cell wall thickening, and pectin modifications. The primary
648 cell wall consists of cellulose and hemicellulose, embedded in a pectin rich matrix (Cosgrove,
649 2024), whereas the secondary cell wall can be further stiffened by lignin deposition. Cell wall
650 stretching and thinning enables the growth of a plant cell which depends on the mechanical
651 strength and dynamic extensibility of the wall. The strength and integrity of the wall is
652 maintained actively by the synthesis and modification of the cell wall elements (Cosgrove,
653 2024; Peaucelle et al., 2011). Histochemical staining revealed increased pectin and lignin
654 accumulation in the palisade layer of high temperature-developed seed coats. Consistently,
655 immunolocalisation using pectin-specific antibodies, together with cell wall profiling of early
656 maturing seed coat, further demonstrated alterations in overall pectin composition,
657 particularly in the palisade layer. Because the degree and pattern of pectin
658 methylesterification influence cell wall rheology, these changes are likely to affect mechanical
659 properties. Pectin, particularly its homogalacturonan (HG) subunit, undergoes dynamic
660 methylesterification and demethylesterication, processes that regulate wall extensibility (Du
661 et al., 2022; D. Wang et al., 2025). The increased abundance of blockwise demethylesterified
662 HG in the palisade layer at 14 and 18 DAP suggests enhanced Ca^{2+}-mediated cross-linking,
663 leading to cell wall stiffening and restricted cell expansion. This stiffening may explain why
664 temperature-accelerated embryo growth was not accompanied by a proportional increase in
665 overall seed size.
666 Nanoindentation analyses of mature seeds provided further insight into the mechanical
667 properties of the seed coat cell walls. Seeds developed under elevated temperature exhibited
668 a lower elastic modulus, indicating that the seed coat cell walls are stiffer and less elastic,
669 which correlates with our finding of reduced degree of pectin methylesterification in the seed
670 coats. Together, these findings indicate that high temperature results in a mechanically stiffer
671 seed coats in HT-grown seed that are less prone to deform than CT-grown seeds.

672 Although elevated temperature promoted accelerated embryo growth and was associated
673 with mechanosensitive accumulation of demethylesterified pectin in the seed coat cell -
674 changes typically linked to increased wall rigidity - this stiffening was insufficient to constrain
675 embryo expansion. Consequently, the structurally weakened and thinner seed coat lacked the
676 extensibility and mechanical strength required to counterbalance the pressure exerted by the
677 rapidly developing embryo. This mechanical imbalance likely culminated in seed coat rupture
678 (SCR). Consistently, physical restriction of seed growth was previously shown to trigger seed
679 maturation by arresting embryonic growth in *B. napus* cv. Reston (Rolletschek et al., 2024).
680 Similar tubing experiments demonstrated that restricting embryo growth while promoting
681 formation of a thicker palisade layer rescued the SCR phenotype further substantiate our
682 hypothesis.
683 These results highlight how high temperature perturbs the biomechanical coordination
684 between embryo growth and seed coat resistance, with important consequences for seed
685 coat integrity.
686
687 **ACKNOWLEDGEMENTS**
688 This work was financially supported by the project TowArds Next GENeration Crops, reg. no.
689 CZ.02.01.01/00/22_008/0004581 of the ERDF Programme Johannes Amos Comenius. We
690 acknowledge the Bioinformatics (supported by the NCLG research infrastructure LM2023067
691 funded by MEYS CR), Cell Imaging (supported by MEYS CR LM2023050 Czech-BioImaging), and
692 Plant Sciences Core Facilities of CEITEC Masaryk University for their support in obtaining the
693 scientific data presented in this paper. This work has benefited from the support of IJPB's
694 Plant Observatory platforms Po-Chem. The IJPB benefits from the support of Saclay Plant
695 Sciences SPS (ANR-17-EUR-0007). This work was also supported by a grant from the French
696 ANR (MECHASEED, ANR-23-CE13-0009) to BL. The nanoindentation tests were supported by
697 the project LM2023039, funded by the Ministry of Education, Youth and Sports of the Czech
698 Republic.
699
700 **COMPETING INTERESTS**
701 The authors declare no competing interests.
702
703 **AUTHOR CONTRIBUTIONS**

704 HSR secured the funding. UP and HSR conceived the project, designed the experiments, and
705 interpreted the data. UP performed the seed phenotyping, histology, transcriptomics, and
706 immunolabelling of the seed coat. IU and JH optimised the protocol for Technovit embedding
707 of oilseed rape seed and prepared the slides for histology. AMM analysed the transcriptomic
708 data. AC, UP, and BL performed the immunolabelling of the seed coat. AV performed the cell
709 wall profiling. VB and UP optimised the nanoindentation of Topas seeds. UP and HSR drafted
710 the manuscript. All authors have proofed and approved the manuscript.
711

712 **DATA AVAILABILITY**

713 The raw data generated during the current study and analysed in this published article (and
714 its Supporting Information file) are available in the Zenodo repository (DOI:
715 10.5281/zenodo.19231242). The dataset supporting the conclusions of this article is
716 deposited to the NCBI repository (BioProject accession number PRJNA1188476,
717 https://www.ncbi.nlm.nih.gov/bioproject/PRJNA1188476).

718

719 **REFERENCES**

720 Agnolucci, P., & De Lipsis, V. (2020). Long-run trend in agricultural yield and climatic factors
721 in Europe. *Climatic Change*, *159*(3), 385–405. https://doi.org/10.1007/s10584-019-
722 02622-3

723 Agnolucci, P., Rapti, C., Alexander, P., De Lipsis, V., Holland, R. A., Eigenbrod, F., & Ekins, P.
724 (2020). Impacts of rising temperatures and farm management practices on global yields
725 of 18 crops. *Nature Food*, *1*(9), 562–571. https://doi.org/10.1038/s43016-020-00148-x

726 Andrews, S. (2010). *FastQC: A Quality Control Tool for High Throughput Sequence Data*.
727 http://www.bioinformatics.babraham.ac.uk/projects/fastqc/

728 Ayala Soto, F. E., & Serna Saldívar, S. O. (2020). *Architecture, Structure and Chemistry of*
729 *Plant Cell Walls and Their Constituents* (pp. 3–14). https://doi.org/10.1007/978-3-030-
730 38654-2_1

731 Bidhendi, A. J., & Geitmann, A. (2016). Relating the mechanics of the primary plant cell wall
732 to morphogenesis. *Journal of Experimental Botany*, *67*(2), 449–461.
733 https://doi.org/10.1093/jxb/erv535

734 Bolger, A. M., Lohse, M., & Usadel, B. (2014). Trimmomatic: a flexible trimmer for Illumina
735 sequence data. *Bioinformatics*, *30*(15), 2114–2120.
736 https://doi.org/10.1093/bioinformatics/btu170

Bond, J., Donaldson, L., Hill, S., & Hitchcock, K. (2008). Safranine fluorescent staining of wood cell walls. *Biotechnic & Histochemistry*, *83*(3–4), 161–171. https://doi.org/10.1080/10520290802373354

Broad Institute, & GitHub Repository. (2018). *Picard Toolkit*. http://broadinstitute.github.io/picard

Chu, J., Sadeghi, S., Raymond, A., Jackman, S. D., Nip, K. M., Mar, R., Mohamadi, H., Butterfield, Y. S., Robertson, A. G., & Birol, I. (2014). BioBloom tools: fast, accurate and memory-efficient host species sequence screening using bloom filters. *Bioinformatics*, *30*(23), 3402–3404. https://doi.org/10.1093/bioinformatics/btu558

Cosgrove, D. J. (2024). Structure and growth of plant cell walls. *Nature Reviews Molecular Cell Biology*, *25*(5), 340–358. https://doi.org/10.1038/s41580-023-00691-y

Creff, A., Ali, O., Bied, C., Bayle, V., Ingram, G., & Landrein, B. (2023). Evidence that endosperm turgor pressure both promotes and restricts seed growth and size. *Nature Communications*, *14*(1). https://doi.org/10.1038/s41467-022-35542-5

Creff, A., Brocard, L., & Ingram, G. (2015). A mechanically sensitive cell layer regulates the physical properties of the Arabidopsis seed coat. *Nature Communications*, *6*. https://doi.org/10.1038/ncomms7382

Dobin, A., Davis, C. A., Schlesinger, F., Drenkow, J., Zaleski, C., Jha, S., Batut, P., Chaisson, M., & Gingeras, T. R. (2013). STAR: ultrafast universal RNA-seq aligner. *Bioinformatics*, *29*(1), 15–21. https://doi.org/10.1093/bioinformatics/bts635

Du, J., Anderson, C. T., & Xiao, C. (2022). Dynamics of pectic homogalacturonan in cellular morphogenesis and adhesion, wall integrity sensing and plant development. *Nature Plants*, *8*(4), 332–340. https://doi.org/10.1038/s41477-022-01120-2

Ewels, P., Magnusson, M., Lundin, S., & Käller, M. (2016). MultiQC: summarize analysis results for multiple tools and samples in a single report. *Bioinformatics*, *32*(19), 3047–3048. https://doi.org/10.1093/bioinformatics/btw354

Figueiredo, D. D., Batista, R. A., Roszak, P. J., Hennig, L., & Köhler, C. (2016). Auxin production in the endosperm drives seed coat development in Arabidopsis. *ELife*, *5*. https://doi.org/10.7554/eLife.20542

Garcia, D., Fitz Gerald, J. N., & Berger, F. (2005). Maternal Control of Integument Cell Elongation and Zygotic Control of Endosperm Growth Are Coordinated to Determine Seed Size in Arabidopsis. *The Plant Cell*, *17*(1), 52–60. https://doi.org/10.1105/tpc.104.027136

Geitmann, A., & Ortega, J. K. E. (2009). Mechanics and modeling of plant cell growth. *Trends in Plant Science*, *14*(9), 467–478. https://doi.org/10.1016/j.tplants.2009.07.006

Haughn, G., & Chaudhury, A. (2005). Genetic analysis of seed coat development in Arabidopsis. In *Trends in Plant Science* (Vol. 10, Number 10, pp. 472–477). https://doi.org/10.1016/j.tplants.2005.08.005

Heino, M., Kinnunen, P., Anderson, W., Ray, D. K., Puma, M. J., Varis, O., Siebert, S., & Kummu, M. (2023). Increased probability of hot and dry weather extremes during the growing season threatens global crop yields. *Scientific Reports*, *13*(1), 3583. https://doi.org/10.1038/s41598-023-29378-2

Jägermeyr, J., Müller, C., Ruane, A. C., Elliott, J., Balkovic, J., Castillo, O., Faye, B., Foster, I., Folberth, C., Franke, J. A., Fuchs, K., Guarin, J. R., Heinke, J., Hoogenboom, G., Iizumi, T., Jain, A. K., Kelly, D., Khabarov, N., Lange, S., … Rosenzweig, C. (2021). Climate impacts on global agriculture emerge earlier in new generation of climate and crop models. *Nature Food*, *2*(11), 873–885. https://doi.org/10.1038/s43016-021-00400-y

Jiang, Y., & Deyholos, M. K. (2010). Transcriptome analysis of secondary-wall-enriched seed coat tissues of canola (Brassica napus L.). *Plant Cell Reports*, *29*(4), 327–342. https://doi.org/10.1007/s00299-010-0824-x

Kassambara, A. (2018). *"ggpubr:'ggplot2' based publication ready plots." R package version 0.17*.

Kolde, R. (2015). *Package 'pheatmap'. R Package 1.7* .

Lapointe, B. P., Kaur, N. S., Routier-Kierzkowska, A.-L., & Burian, A. (2025). From stress to growth: Mechanical tissue interactions in developing organs. *Current Opinion in Plant Biology*, *86*, 102759. https://doi.org/10.1016/j.pbi.2025.102759

Lenssen, N., Schmidt, G. A., Hendrickson, M., Jacobs, P., Menne, M. J., & Ruedy, R. (2024). A NASA GISTEMPv4 Observational Uncertainty Ensemble. *Journal of Geophysical Research: Atmospheres*, *129*(17). https://doi.org/10.1029/2023JD040179

Li, N., Xu, R., & Li, Y. (2019). Molecular Networks of Seed Size Control in Plants. *Annual Review of Plant Biology*, *70*(1), 435–463. https://doi.org/10.1146/annurev-arplant-050718-095851

Liao, Y., Smyth, G. K., & Shi, W. (2014). featureCounts: an efficient general purpose program for assigning sequence reads to genomic features. *Bioinformatics*, *30*(7), 923–930. https://doi.org/10.1093/bioinformatics/btt656

Lima, R. B., Pankaj, R., Ehlert, S. T., Finger, P., Fröhlich, A., Bayle, V., Landrein, B., Sampathkumar, A., & Figueiredo, D. D. (2024). Seed coat-derived brassinosteroid signaling regulates endosperm development. *Nature Communications*, *15*(1), 9352. https://doi.org/10.1038/s41467-024-53671-x

Love, M. I., Huber, W., & Anders, S. (2014). Moderated estimation of fold change and dispersion for RNA-seq data with DESeq2. *Genome Biology*, *15*(12), 550. https://doi.org/10.1186/s13059-014-0550-8

Mácová, K., Prabhullachandran, U., Štefková, M., Spyroglou, I., Pěnčík, A., Endlová, L., Novák, O., & Robert, H. S. (2022). Long-Term High-Temperature Stress Impacts on Embryo and Seed Development in Brassica napus. *Frontiers in Plant Science*, *13*. https://doi.org/10.3389/fpls.2022.844292

Marin-Rodriguez, M. C. (2002). Pectate lyases, cell wall degradation and fruit softening. *Journal of Experimental Botany*, *53*(377), 2115–2119. https://doi.org/10.1093/jxb/erf089

Mendu, V., Griffiths, J. S., Persson, S., Stork, J., Downie, A. B., Voiniciuc, C., Haughn, G. W., & DeBolt, S. (2011). Subfunctionalization of Cellulose Synthases in Seed Coat Epidermal Cells Mediates Secondary Radial Wall Synthesis and Mucilage Attachment . *Plant Physiology*, *157*(1), 441–453. https://doi.org/10.1104/pp.111.179069

Mohnen, D. (2008). Pectin structure and biosynthesis. *Current Opinion in Plant Biology*, *11*(3), 266–277. https://doi.org/10.1016/j.pbi.2008.03.006

Nagayama, T., Nakamura, A., Yamaji, N., Satoh, S., Furukawa, J., & Iwai, H. (2019). Changes in the Distribution of Pectin in Root Border Cells Under Aluminum Stress. *Frontiers in Plant Science*, *10*. https://doi.org/10.3389/fpls.2019.01216

NASA Goddard Institute for Space Studies. (2026, March 2). https://data.giss.nasa.gov/gistemp/

Okonechnikov, K., Conesa, A., & García-Alcalde, F. (2016). Qualimap 2: advanced multi-sample quality control for high-throughput sequencing data. *Bioinformatics*, *32*(2), 292–294. https://doi.org/10.1093/bioinformatics/btv566

Oliver, W. C., & Pharr, G. M. (1992). An improved technique for determining hardness and elastic modulus using load and displacement sensing indentation experiments. *Journal of Materials Research*, *7*(6), 1564–1583. https://doi.org/10.1557/JMR.1992.1564

Park, K.-C., Kwon, S.-J., & Kim, N.-S. (2010). Intron loss mediated structural dynamics and functional differentiation of the polygalacturonase gene family in land plants. *Genes & Genomics*, *32*(6), 570–577. https://doi.org/10.1007/s13258-010-0076-8

Peaucelle, A., Braybrook, S. A., Le Guillou, L., Bron, E., Kuhlemeier, C., & Höfte, H. (2011). Pectin-Induced Changes in Cell Wall Mechanics Underlie Organ Initiation in Arabidopsis. *Current Biology*, *21*(20), 1720–1726. https://doi.org/10.1016/j.cub.2011.08.057

Rolletschek, H., Muszynska, A., Schwender, J., Radchuk, V., Heinemann, B., Hilo, A., Plutenko, I., Keil, P., Ortleb, S., Wagner, S., Kalms, L., Gündel, A., Shi, H., Fuchs, J., Szymanski, J. J., Braun, H., & Borisjuk, L. (2024). Mechanical forces orchestrate the metabolism of the developing oilseed rape embryo. *New Phytologist*, *244*(4), 1328–1344. https://doi.org/10.1111/nph.19990

Safran, J., Tabi, W., Ung, V., Lemaire, A., Habrylo, O., Bouckaert, J., Rouffle, M., Voxeur, A., Pongrac, P., Bassard, S., Molinié, R., Fontaine, J.-X., Pilard, S., Pau-Roblot, C., Bonnin, E., Larsen, D. S., Morel-Rouhier, M., Girardet, J.-M., Lefebvre, V., … Pelloux, J. (2023). Plant polygalacturonase structures specify enzyme dynamics and processivities to fine-tune cell wall pectins. *The Plant Cell*, *35*(8), 3073–3091. https://doi.org/10.1093/plcell/koad134

Secchi, M. A., Fernandez, J. A., Stamm, M. J., Durrett, T., Prasad, P. V. V., Messina, C. D., & Ciampitti, I. A. (2023). Effects of heat and drought on canola (Brassica napus L.) yield, oil, and protein: A meta-analysis. *Field Crops Research*, *293*, 108848. https://doi.org/10.1016/j.fcr.2023.108848

Sechet, J., Marion-Poll, A., & North, H. M. (2018). Emerging Functions for Cell Wall Polysaccharides Accumulated during Eudicot Seed Development. *Plants*, *7*(4), 81. https://doi.org/10.3390/plants7040081

Turbant, A., Fournet, F., Lequart, M., Zabijak, L., Pageau, K., Bouton, S., & Van Wuytswinkel, O. (2016). PME58 plays a role in pectin distribution during seed coat mucilage extrusion through homogalacturonan modification. *Journal of Experimental Botany*, *67*(8), 2177–2190. https://doi.org/10.1093/jxb/erw025

Voxeur, A., Habrylo, O., Guénin, S., Miart, F., Soulié, M.-C., Rihouey, C., Pau-Roblot, C., Domon, J.-M., Gutierrez, L., Pelloux, J., Mouille, G., Fagard, M., Höfte, H., & Vernhettes, S. (2019). Oligogalacturonide production upon *Arabidopsis thaliana – Botrytis cinerea* interaction. *Proceedings of the National Academy of Sciences*, *116*(39), 19743–19752. https://doi.org/10.1073/pnas.1900317116

Wang, D., Ortega-Salazar, I. B., & Blanco-Ulate, B. (2025). Homogalacturonan Methylesterification and Cell Wall Regulation: Integrating Biochemistry, Mechanics, and Developmental Signaling for Crop Improvement. *Agronomy*, *15*(11), 2641. https://doi.org/10.3390/agronomy15112641

Wang, L., Wang, S., & Li, W. (2012). RSeQC: quality control of RNA-seq experiments. *Bioinformatics*, *28*(16), 2184–2185. https://doi.org/10.1093/bioinformatics/bts356

Wickham, H. (2011). ggplot2. *WIREs Computational Statistics*, *3*(2), 180–185. https://doi.org/10.1002/wics.147

Wormit, A., & Usadel, B. (2018). The Multifaceted Role of Pectin Methylesterase Inhibitors (PMEIs). *International Journal of Molecular Sciences*, *19*(10), 2878. https://doi.org/10.3390/ijms19102878

Wu, H.-C., Bulgakov, V. P., & Jinn, T.-L. (2018). Pectin Methylesterases: Cell Wall Remodeling Proteins Are Required for Plant Response to Heat Stress. *Frontiers in Plant Science*, *9*, 1612. https://doi.org/10.3389/fpls.2018.01612

Xu, Z., Yang, M., Li, Z., Xiao, J., Yang, X., Wang, H., & Wang, X. (2022). Tissue-specific pectin methylesterification and pectin methylesterase activities play a role in lettuce seed germination. *Scientia Horticulturae*, *301*, 111134. https://doi.org/10.1016/j.scienta.2022.111134

Young, L. W., Wilen, R. W., & Bonham-Smith, P. C. (2004). High temperature stress of Brassica napus during flowering reduces micro- and megagametophyte fertility, induces fruit abortion, and disrupts seed production. *Journal of Experimental Botany*, *55*(396), 485–495. https://doi.org/10.1093/jxb/erh038

889 Zhao, C., Liu, B., Piao, S., Wang, X., Lobell, D. B., Huang, Y., Huang, M., Yao, Y., Bassu, S.,
890 Ciais, P., Durand, J. L., Elliott, J., Ewert, F., Janssens, I. A., Li, T., Lin, E., Liu, Q., Martre,
891 P., Müller, C., … Asseng, S. (2017). Temperature increase reduces global yields of major
892 crops in four independent estimates. *Proceedings of the National Academy of Sciences*
893 *of the United States of America*, *114*(35), 9326–9331.
894 https://doi.org/10.1073/pnas.1701762114

895

896 **FIGURE LEGENDS**

897 **Fig. 1.** SCR phenotype observed in Topas seeds developed under HT. (a) 26 DAP seeds and
898 matured dry seeds after harvest grown under CT. (b) 26 DAP seeds and matured dry seeds
899 after harvest grown under HT depicting the seed coat rupture (SCR); on the left are seeds with
900 incomplete testa rupture and on the right, seeds with fully ruptured seed coat with protruding
901 embryos. (c) Quantification of the percentage of dry seeds per silique from CT (blue) and HT
902 (red) showing the percent of intact, SCR and dead seeds (n CT= 116, n HT= 245). Phenotypic
903 classification represented in Fig. S1a-c. Asterisks indicate statistically significant differences in
904 HT in a multiple t-test using the Holm-Sidak method (**** corresponds to *p*-values of $p <$
905 0.0001. (d) Embryo stage of seeds developed on CT (top) and HT (bottom) from 14 to 20 DAP.
906 The isolated embryo shown on the right is from the seed on the left. Scale bars: 1 mm (a,b)
907 and 3mm (d).

908

909 **Fig. 2.** Embryo and seed size measurements of *Brassica napus* cv. Topas seeds developed at
910 CT and HT. (a, b) Embryo (a) and seed (b) area measurements in mm^2 of 14, 18 and 20 DAP
911 Topas seeds developed at CT (blue) and HT (red). (c) Ratio of embryo-to-seed size 14, 18 and
912 20 DAP Topas seeds developed at CT and HT. Asterisks indicate statistically significant
913 differences in HT and between 14 DAP HT and 18 DAP CT in a two-way ANOVA test with
914 Sidak's multiple comparisons (*, **, *** and **** correspond to *p*-values of $0.05 > p > 0.005$,
915 $0.005 > p > 0.0005$, $0.0005 > p > 0.0005$ and $p < 0.00005$, respectively); n.s., not significant.
916 (d) Upregulated GO terms ($Log_2FC \geq 1.32$) related to plant development with the
917 transcriptional response of Topas seeds to HT (values in the box depict $-log_{10}$q-value).

918

919 **Fig 3.** The thickness of the seed coat cells is reduced in HT. (a-e) Histological sections of Topas
920 seeds focused on the seed coat, stained with toluidine blue. (a) The seed coat is composed of
921 an epidermal layer, a palisade layer and an endodermal layer. (b-e) Seed coat of 14 DAP seeds

922 from CT (b) and HT (d) and 18 DAP seeds from CT (c) and HT (e). Scale bars represent 200 µm.
923 (f-h) Box-whisker plots show the size mean, median, outliers, and SD in µm of the thickness
924 of the epidermal layer (f), palisade layer (g) and first endothelial cell layer (h) in 10, 14, 18,
925 and 20 DAP seeds from CT (blue) and HT (red). Samples with the same letter were not
926 statistically significantly different. (i) Percentage of reduction in thickness as the seed aged
927 from 14 to 20 DAP.
928
929 **Fig.4.** Transcriptional changes in Topas seeds associated with growth at HT indicate changes
930 in cell wall composition. (a) GO terms associated to cell wall metabolism and regulation with
931 the transcriptional response of Topas seeds to HT are shown (values in the box depict $-\log_{10}$q-
932 value). (b) Heatmap showing the differential transcription of selected genes involved in pectin
933 metabolism in 14 DAP HT vs 18 DAP CT seeds (A), and SCR vs non-SCR seeds (B) at 20 DAP
934 from HT. The full dataset is presented in Tables S1 and S2. (c) Histological sections of Topas
935 seeds focused on the seed coat, stained with Ruthenium Red for pectin. Sections of 14, 18,
936 and 22 DAP CT seeds and 14 and 18 DAP HT seeds are shown. Scale bars represent 200 µm.
937
938 **Fig. 5** Immunolocalization to estimate the degree of pectin methylation using LM19, JIM5,
939 and LM20 antibodies on the seed coat of 14 and 18 DAP CT and HT seeds. The signal is visible
940 in green; the cell structure is marked in magenta with calcofluor white. Scale bars represent
941 100 µm. Fluorescence intensity was measured in epidermal and palisade cells in 10, 14 and
942 18 DAP HT and CT seeds. Asterisks indicate statistically significant differences in HT and
943 between seed ages in a one-way ANOVA test with Tukey multiple comparisons (*, **, *** and
944 **** correspond to p-values of $0.05 > p > 0.01$, $0.01 > p > 0.001$, $0.001 > p > 0.0001$ and $p <$
945 0.0001, respectively); n.s., not significant.
946
947 **Fig. 6** Pectin enzymatic profiling. (a) Pectin composition of the seed coat cell wall of 10, 14,
948 and 18 DAP seeds from HT and CT. The graph shows the measurements expressed as peak
949 area from the MS analysis for GalA3, GalA3ox, GalA3Xyl, GalA3Me, GalA3MeAc, GalA4Ac,
950 GalA4Me, GalA4Meox, GalA4Me-H_2O and DPx>4Mey (methylesterified OGs with degree of
951 polymerisation greater than 4). (b) Graph showing the amount grouped as methylesterified
952 versus non-methylesterified OGs from (c) Graph showing the total intensity signal for pectin
953 from (Fig. 5).

954

955 **Fig. 7** Seed coat mechanobiology of *B. napus* seeds. (a) Measurement of elastic modulus, E_r
956 (MPa) comparing 20 and 24 DAP seeds from CT and HT respectively. (b) A 3-mm silicon tube
957 was applied to siliques from 10 DAP CT and 12 DAP HT. Dry seeds were quantified for the
958 percent of intact, SCR and dead seeds per silique. Asterisks indicate statistically significant
959 differences in HT and between seed ages in a two-way ANOVA test with Tukey multiple
960 comparisons (*, **, *** and **** correspond to *p*-values of $0.05 > p > 0.01$, $0.01 > p > 0.001$,
961 and $p < 0.001$, respectively); n.s., not significant. (d,e) Box-whisker plots show the size,
962 median, outliers, and SD in µm of the thickness of the epidermal layer (c), palisade layer (d)
963 of seeds at 24 DAP from CT and 20 DAP from HT to account for same developmental stage.

964

965 **SUPPORTING INFORMATION**

966 Additional Supporting Information may be found online in the Supporting Information section
967 at the end of the article.

968 **Fig. S1** Representation of seed phenotyping strategy in Brassica napus (Topas).

969 **Fig. S2** Principal component analysis using gene expression data from the samples tested for
970 differences between samples and biological replicates.

971 **Fig. S3** Upregulated GO terms ($Log_2FC \geq 1$) related to cell cycle regulation with the
972 transcriptional response of Topas seeds to HT (values in the box depict $-log_{10}$q-value).

973 **Fig. S4** Histological sections of Topas seeds focused on the seed coat, stained with Safranin-O
974 for lignin.

975 **Fig. S5** Quantification of xyloglucans in the Topas seed coat.

976 **Fig. S6** Silicone tube mediated space restricted growth of seeds.

977 **Fig. S7** Representative images of the 3-D printed mould for immobilizing the seed during
978 nanoindentation.

979 **Fig. S8** Represents the number of shared downregulated DEGs

980 **Fig. S9** Represents the number of shared upregulated DEGs

981 **Table S1** Full dataset for the DEGs for all the comparisons.

982 **Table S2** Misregulated GO terms associated with plant cell wall, cell cycle, heat response and
983 developmental pathways.